Inner–outer interactions in a turbulent boundary layer overlying complex roughness

Gokul Pathikonda and Kenneth T. Christensen

Inner–outer interactions in a turbulent boundary layer overlying complex roughness

Gokul Pathikonda
Department of Mechanical Science and Engineering,
University of Illinois, Urbana-Champaign, USA and
Aerospace and Mechanical Engineering, University of Notre Dame, Notre Dame, USA

Kenneth T. Christensen*
Aerospace and Mechanical Engineering; Civil & Environmental Engineering & Earth Sciences,
University of Notre Dame, Notre Dame, USA and
International Institute for Carbon-Neutral Energy Research, Kyushu University, Fukuoka, Japan

Hot-wire measurements were performed in a zero-pressure-gradient turbulent boundary layer overlying both a smooth and a rough wall for the purpose of investigating the details of inner–outer flow interactions. The roughness considered embodies a broad range of topographical scales arranged in an irregular manner and reflects the topographical complexity often encountered in practical flow systems. Single-probe point-wise measurements with a traversing probe were made at two different regions of the rough-wall flow, which was previously shown to be heterogeneous in the spanwise direction, to investigate the distribution of streamwise turbulent kinetic energy and large scale–small scale interactions. In addition, two-probe simultaneous measurements were conducted enabling investigation of inner–outer interactions wherein the large scales were independently sampled in the outer layer. Roughness-induced changes to the near-wall behavior were investigated, particularly by contrasting the amplitude and frequency modulation effects of inner–outer interactions in the rough-wall flow with well-established smooth-wall flow phenomena. It was observed that the rough-wall flow exhibits both amplitude and frequency modulation features close to the wall in a manner very similar to smooth-wall flow, though the correlated nature of these effects was found to be more intense in the rough-wall flow. In particular, frequency modulation was found to illuminate these enhanced modulation effects in the rough-wall flow. The two-probe measurements helped in evaluating the suitability of the interaction-schematic recently proposed by Baars *et al.* [1] for rough-wall flows. This model was found to be suitable for the rough-wall flow considered herein and it was found that frequency modulation is a 'cleaner' measure of the inner–outer modulation interactions for this rough-wall flow.

* christensen.33@nd.edu

I. INTRODUCTION

An incompressible smooth-wall turbulent boundary layer at 'sufficiently' high Reynolds number (Re) can be, broadly speaking, divided into three regions: (1) an inner, near-wall, turbulence-generating region, (2) an outer wake region, and (3) an inertial region in-between where both the outer and inner formulations are asymptotically and simultaneously valid. It can be argued that the near-wall dynamics are primarily dependent only on the near-wall conditions, and thus must be fully represented by the same, i.e., wall shear stress (τ_w) and kinematic viscosity (ν). Similarly, the outer layer dynamics must be defined primarily by velocity difference from the free-stream velocity (U_∞) and outer length scale (δ, the boundary-layer thickness), or equivalently Re. These two mechanisms must then be matched by a universal region in which both regions asymptotically approach and match. For many turbulent flow hypotheses, the 'sufficiency' of high Re is qualified by the existence and extent of such a universal region in the flow. This region, termed the '*inertial region*', can be viewed as the energy pathway between the demanding inner region and supplying outer region, operated by a cascade of energy-containing eddy scales. It must be remembered that this simplified description of a wall-bounded turbulent flow is valid in an average sense, and does not necessarily depict the instantaneous dynamics. An elaborated description and early experimental evidence for this perception of smooth-wall turbulent boundary layers can be found, for example, in Clauser [2].

The turbulence-generating, near-wall region of smooth-wall flow has been observed to be populated by structures of quasi-streamwise-oriented vortices [3]. These structures were found to scale well with the inner scales of wall shear stress and viscosity, and have been proposed to form a self-sustaining, turbulence-generating mechanism [4, 5]. They had long been assumed to be dynamically independent of Re, as shown by simple scaling arguments, via the apparent invariance of the near-wall turbulent kinetic energy (TKE) peak in early hot-wire measurements and DNS simulations of such flows.

More recently, Kim and Adrian [6] observed significant TKE content ('outer peaks') in the inertial region of smooth-wall pipe flow at much larger streamwise scales ($\lambda > \delta$). These motions were categorized as 'large-' ($\lambda_x < 3\delta$) and 'very-large-scale motions' ($\lambda_x > 3\delta$) [7] – LSMs and VLSMs, respectively. Their influence appeared in pre-multiplied spectral energy maps as a secondary TKE peak near the geometric center of the log region [8], and at streamwise length scales $\sim O(10\delta)$ [7], where δ is the outer length scale (the boundary-layer thickness, pipe radius or channel half-height). Similar observations of energetic motions at long streamwise scales have been made in turbulent channel flow [7] and turbulent boundary layers [9], with the VLSMs also termed as 'superstructures'. Particle-image velocimetry (PIV) measurements established the structural characteristics of LSMs [10], and the dynamic significance of these superstructures as influential contributors to local Reynolds shear stress [11] and momentum transport [12]. Sufficiently long hot-wire rake measurements were made to establish the spanwise and streamwise characteristics of superstructures by Hutchins and Marusic [9]–both statistically and instantaneously–as they far exceed the field of view of PIV measurements.

As the energy content of these large- and very-large-scale motions grows with Re, it is reasonable to expect that they might begin to interact with the autonomous near-wall region in high-Re smooth-wall flow [13]. Early observations by Rao *et al.* [14] revealed such outer-scale influences on the near-wall cycle as the near-wall bursting phenomenon was found to scale with outer scales. A clear amplitude modulation of the near-wall structures by the outer-scale superstructures was experimentally observed by Bandyopadhyay and Hussain [15] and Mathis *et al.* [16], thus establishing a definitive interaction and linkage between the outer and inner regions of smooth-wall flow. Particularly, correlations between the large scales and the filtered envelope of small scales (determined using the Hilbert transform) show that that a 'positive' large-scale event in the logarithmic region is typically associated with an increase in the amplitude of the small scales, and vice versa [16]. These interaction correlations were then used by Mathis *et al.* [17] and Marusic *et al.* [18] to develop a model that successfully predicted a range of near-wall turbulence statistics. Mathis *et al.* [19] and Duvvuri and McKeon [20] deconstructed the contributions of various terms in velocity skewness, and their relation with the amplitude modulation correlation coefficient, while Bernardini and Pirozzoli [21] showed amplitude modulation interactions in DNS simulations via two-point correlations. Guala *et al.* [22] showed changes in conditional average of energy spectra at small scales between the high- and low-speed large-scale events in atmospheric boundary layer.

With the existence of inner–outer interactions in smooth-wall flow clearly established, recent studies have investigated this relation between the large and small scales in aforementioned regions of the flow in more detail. In the logarithmic region of a smooth-wall turbulent boundary layer, Chung and McKeon [23] and Hutchins *et al.* [24] used conditional averaging to investigate small-scale activity around large-scale events using LES and experiments, respectively. The strong correlation between the streamwise gradient of large-scale velocity and the small-scale amplitude variations has been hypothesized to be from spanwise-meandering of the aforementioned superstructures. A similar correlation analysis in spectral space via the co-spectral densities was performed by Jacobi and McKeon [25]. In addition to the modulation of the streamwise velocity scales, the spanwise and wall-normal velocity components have also been shown to exhibit similar modulation phenomena [26]. The wall shear stress has also been observed by

Mathis *et al.* [27] to be experiencing such influences, and a predictive model (along the lines of Mathis *et al.* [17]) was proposed to predict the same. Interestingly, such large- and small-scale interactions are not limited to wall-bounded flows, as similar interactions were reported recently in jet flows [28].

Besides amplitude modulation, frequency modulation (FM) of the small scales by the large scales presents another manifestation of inner–outer interactions in wall-bounded flows. Ganapathisubramani *et al.* [29] identified frequency modulation between the small and large scales near the wall, similar to AM interactions. More recently, Baars *et al.* [1] used the continuous wavelet transform to investigate frequency modulation in smooth-wall turbulent boundary layers, and established the existence of FM effects. Further, conditional averages of the wavelet power spectrum provided further insight as to plausible mechanisms of inner–outer interactions, namely as a quasi-steady response of the near-wall region to large-scale changes in the outer flow [1, 30]. A theoretical framework for this idea was given by Zhang and Chernyshenko [31] as a "Quasi-Steady, Quasi Homogenous (QSQH)" response of the near-wall structures to the large-scale fluctuations in the outer layer.

With a fundamental framework of inner–outer interactions firmly established in smooth-wall flows, it is of interest to explore whether similar interactions occur in rough-wall flow. A rough-wall turbulent boundary layer at high Re and subjected to a relatively "small" wall roughness height, k (i.e., small relative to $\delta/k \gg 1$) bears dynamical similarity to its smooth-wall counterpart in many ways. Townsend's attached eddy hypothesis [32] states that the outer region of the boundary layer remains identical, with the near-wall turbulence production cycle in smooth-wall flow being replaced by the a roughness-perturbed layer (termed the roughness sublayer). At high Re and for $\delta/k \gg 1$, the outer layer merely adapts itself to the rough-wall boundary conditions (virtual origin, y_c, friction velocity, u_τ, velocity defect, ΔU, and boundary layer thickness, δ), with the outer-layer turbulent dynamics behaving similar to that of smooth-wall flow [33, 34]. Given similar LSM-VLSM structure in the outer region of such a rough-wall turbulent boundary layer [35, 36], investigating the response of the roughness sublayer to these outer modulating influences is of strong interest, particularly for the development of predictive models similar to that previously developed for smooth-wall flow [17, 18, 27] for the more practically relevant case of rough-wall flow. Squire *et al.* [37] investigated the applicability of the modified model developed by Marusic *et al.* [18] for the case of rough-wall boundary layers, and observed possibly stronger AM (as measured by the model) compared to smooth-wall flow for flow over sandpaper roughness. Blackman and Perret [38] attempted to link the receptivity of shear-layer structures shed by macroscopic roughness to the large scales in the outer layer using PIV measurements and stochastic estimation. Numerically, Nadeem *et al.* [39] and Anderson [40] recently reported AM in flows perturbed by periodic roughness arrays using DNS (two-dimensional rods) and LES (cubes) simulations, respectively. These studies indicate the occurrence of AM in rough-wall flow for cases with simplified roughness topographies, but they have not considered the occurrence nor characteristics of FM in rough-wall flow nor the case of more irregular roughness that is reminiscent of that encountered in practical flow systems.

With this understanding, the current work experimentally examines the strength and robustness of inner–outer interactions in a rough-wall turbulent boundary layer using both AM and FM analysis as well as a complex roughness topography reflective of the irregularity often encountered in pratice. We aim to identify if and how superstructures in the log region of this rough-wall flow (previously identified in Mejia-Alvarez *et al.* [36]) interact with the near-wall velocity perturbations imparted within the roughness sublayer by a multi-scale roughness topography– whose flow behavior has been previously reported [34–36, 41, 42]. The complex roughness used in the current study embodies a broad range of topographical scales and its heterogeneity in the spanwise direction was shown to induce spanwise-alternating, localized, δ-scale high- and low-momentum pathways (HMPs and LMPs, respectively) reflective of roughness-induced turbulent secondary flows [43–45]. Thus, the modulating influences of inner–outer interactions are studied at these localized spanwise conditions induced by the underlying roughness-induced secondary flows.

II. EXPERIMENTS

The experiments that form the current study involve single- and two-point measurements of streamwise velocity over smooth- and rough-wall turbulent boundary layers using constant-temperature hot-wire anemometry (HWA). This section summarizes the flow facility utilized, the roughness employed and details of the HWA measurements.

A. Experimental Facility and Surface Conditions

All experiments were conducted in an open-circuit, Eiffel-type, boundary-layer wind tunnel with a test section having a 0.91 m wide and 0.46 m tall cross section and the boundary layers of interest formed on a 6.1 m long hydraulically smooth flat plate. The flat plate itself is suspended 100 mm above the floor of the wind tunnel, has an elliptic leading edge and a 5 mm cylindrical trip mounted downstream of the leading edge. Twenty equidistant
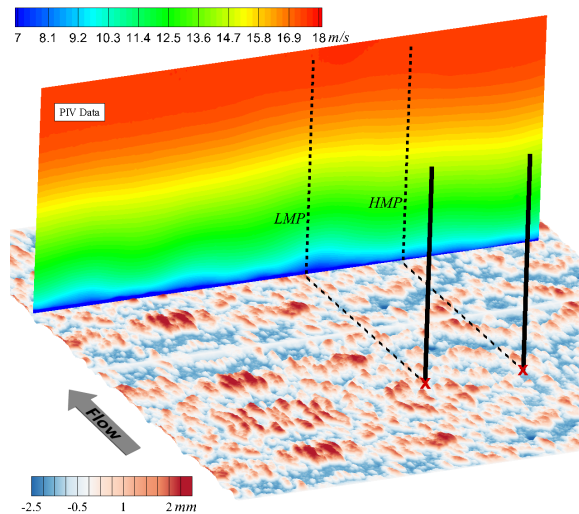
FIG. 1. A true-scale schematic of the hot-wire measurement locations relative to the complex roughness shown in perspective view. The mean streamwise velocity is presented in a cross-flow plane (measured using sPIV), highlighting the spanwise positions of the current hot-wire measurements (denoted with 'X') at an LMP (*left*) and HMP (*right*), as previously identified by Barros and Christensen [43]. The current measurement points are 150 mm upstream of the PIV plane indicated, and distributed on the solid line.

static pressure ports on the plate enabled monitoring of the streamwise pressure variations. Zero-pressure-gradient conditions were maintained for all the boundary layers by contouring the adjustable ceiling of the wind tunnel to maintain pressure variations to less than 1% of the free-stream dynamic head. The free-stream turbulence intensity of the flow, at speeds relevant to this study, were measured to be approximately 0.16%. More details and characteristics of this tunnel can be found in many past studies [46, 47].

The smooth boundary-layer plate was constructed of two separate plates of equal 3 m length, mounted on adjustable screws enabling the two plates to be elevated independently (enabling a forward facing or backward facing step where they meet in the streamwise center of the test section). For all smooth-wall turbulent boundary layer experiments in current study, the plates were kept level with each other, and the boundary layer is allowed to develop for about 6 m to the measurement location. For the rough-wall turbulent boundary layer case, the roughness (mounted on aluminum plates) was placed atop the downstream 3 m section of the boundary-layer plate, and the upstream plate was elevated to be coincident with the mean roughness height of the downstream roughness (i.e., without any forward or backward facing steps). Thus the boundary layer, in this case, initially developed for 3 m over smooth-wall conditions and then developed over the roughness for another 3 m to the measurement location. This arrangement is consistent with past studies of this specific roughness topography that have observed flow features and characteristics relevant to the current study [34, 43], the details of which are elaborated in the following sections.

The rough surface used for the rough-wall turbulent boundary layer experiments was the same as that originally fabricated and studied by Wu and Christensen [34, 35] and Mejia-Alvarez and Christensen [41]. The topography was replicated from a topographical scan of an in-use turbine blade damaged by deposition of materials. This topography has a mean peak-to-valley height of 4.25 mm and a root-mean-square (rms) roughness height of 1.0 mm. Figure 1 shows the roughness topography in perspective view. Further details about the surface, its manufacturing, the roughness' physical characteristics, etc. can be found in previous studies [34, 35, 41].

A note on mean flow characteristics

Outer-layer similarity, which implies the existence of LSM and VLSM dynamics in rough-wall flow that are similar to those in smooth-wall flow, has been well-established by Wu and Christensen [34] and Mejia-Alvarez *et al.* [36]. Hence, they are assumed in the current experiments, which are conducted under identical conditions. Further, the complex topography used in the current study, with a broad range of roughness scales arranged in an irregular manner, also has distinctive large-scale spanwise heterogeneity in roughness height. This large-scale spanwise heterogeneity in the topography has been found to generate alternating high- and low- momentum mean-flow pathways (HMPs and LMPs) of length scale of order δ in the spanwise direction [43, 47]– also shown in Fig. 1. These alternating HMP–LMP pairs were found to sandwich streamwise oriented counter-rotating roll cells and these regions extend at least
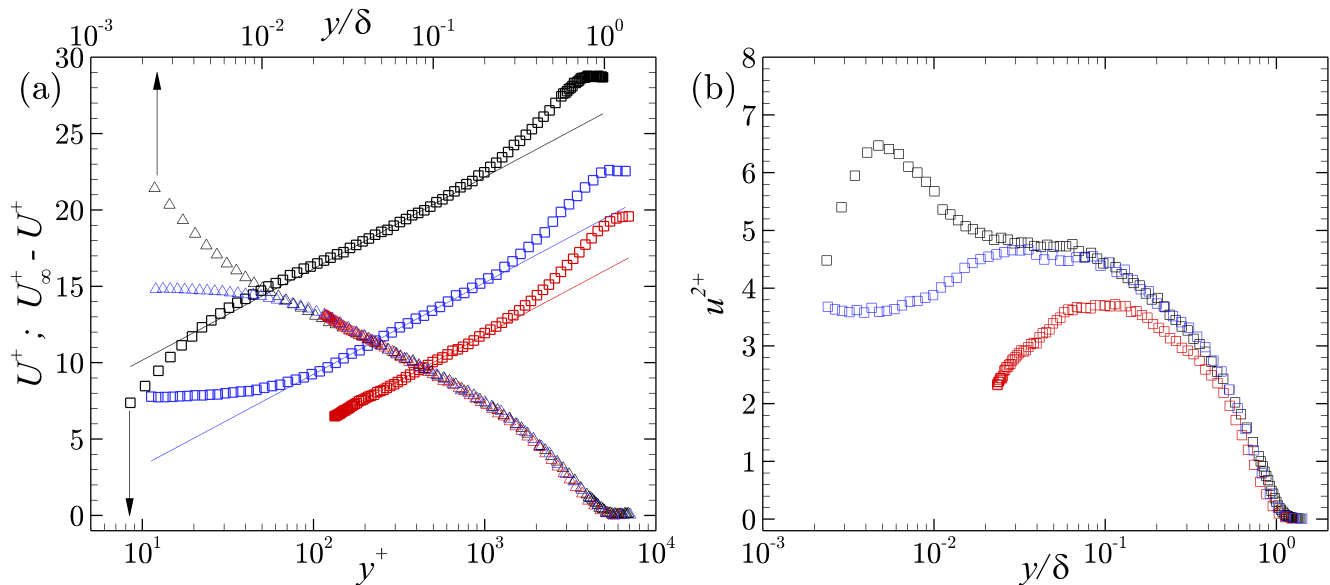
FIG. 2. (a) Profiles of mean velocity normalized in inner units (*squares*), and in defect form with y-normalized in outer units (*triangles*). Also shown are logarithmic profiles with $\kappa = 0.384$. (b) Corresponding mean streamwise turbulent kinetic energy profiles. Smooth; Rough (LMP); Rough (HMP).

δ in the streamwise direction [42]. These mean-flow characteristics are consistent with roughness-induced turbulent secondary flows and subsequent work established that they are indeed secondary flows of the second kind induced by the spanwise heterogeneity of the roughness topography itself [44, 45]. More recently, experiments have identified the formation of similar mean secondary flows for flow over converging-diverging riblet roughness by Nugroho *et al.* [48], Kevin *et al.* [49]. These features are suspected to be a common feature in boundary layers that are exposed to surface roughness with large-scale topographic heterogeneity in the spanwise direction.

Figure 2a shows the mean velocity profiles measured in the current study, indicating the difference between the LMP and HMP regions. These differences are also evident in the mean streamwise turbulent kinetic energy profiles in Fig. 2b, which clearly indicate the higher turbulent kinetic energy in the HMP region compared to the LMP region. This was also found in previous PIV measurements by Barros and Christensen [43]. The boundary layer parameters for the three flows measured can be found in table I.

B.   Hot-Wire Anemometry

Single-component constant temperature hot-wire measurements, made with a Dantec StreamLine 90C10 CTA system and 55P05 boundary-layer probes (1.25 mm length and 5 μm diameter), are presented herein. All measurements were conducted approximately 2.3 m downstream of the leading edge of the roughness. As mentioned before, the rough-wall flow at this measurement location was previously reported [34] to have achieved self-similar conditions, with outer-layer similarity in the mean and turbulence statistics compared to smooth-wall flow at comparable Re.

Before and after each experiment, the hot-wire probe(s) are translated into the free stream and calibrated *in situ* using a pitot-static probe in tandem, and by varying free-stream velocity. Average of the two calibrations for each experiment is used for subsequent conversions of bridge voltage to velocity signal. The maximum drift between the pre- and post-measurement calibrations has been consistently less than 0.1%, indicating the stability of the system. Further, temperature of the free stream flow was measured at 6 Hz, to apply temperature corrections to the hot-wire voltage measurements.

Two separate sets of measurements were performed for each case described in the current study: (a) with a single, wall-normal-traversing probe (termed *1-Probe measurements* henceforth) and (b) with two probes at identical streamwise and spanwise positions making simultaneous measurements, with one probe fixed in the log region $(y_\circ)$ and the other traversing from the wall towards the fixed outer probe (termed *2-Probe measurements*). The 2-probe setup is similar to that reported Mathis *et al.* [17]. First, the 1-probe measurements traversed the entire boundary layer, allowing all relevant parameters of the flow to be determined (u_τ, ΔU, δ, U_∞, etc.). Here, the boundary-layer thickness, δ, is taken as the wall-normal location where the mean streamwise velocity is 99% of U_∞. The two-probe

TABLE I. Experimental parameters.

Flow	Re_τ	U_∞ (m/s)	δ (mm)	u_τ (m/s)	y_* (μm)	ΔU^+	$y_\circ^+$
Smooth	3560	16.61	94.7	0.58	26.6	-	197 $(0.055\delta^+)$
R-LMP	5650	16.94	98.2	0.85	17.6	10.3	726 $(0.14\delta^+)$
R-HMP	4850	17.29	96.6	0.78	20.4	6.9	612 $(0.13\delta^+)$

measurements were then conducted at identical spanwise positions and flow conditions. Both types of measurements were first performed for smooth-wall flow as a means of comparing and confirming the modulation effects with previous literature, as well as a baseline against which the rough-wall data are compared.

Table I summarizes the parameters for the smooth- and rough-wall experiments conducted. The rough-wall measurements were conducted at distinct spanwise positions so that they resided at the spanwise position of an LMP and a HMP, as shown in Fig. 1. It should be noted that the Re of the smooth- and rough-wall flows are slightly different. Mathis *et al.* [16] addressed this issue for smooth-wall flow, and found a few percent increase in the amplitude modulation metric for an approximately 30% difference in Re corresponding to the range of Re considered herein. Thus, small differences in the strength of the inner–outer interactions between smooth- and rough-wall flow are possible due to Re differences, though any larger differences can then be ascribed to roughness effects. A few near-wall points in the smooth-wall measurements were excluded using a diagnostic plot [50]. For rough-wall measurements at the HMP location, some y-locations close to wall were discarded, whose corresponding time-series values fail a minimum-velocity criterion. This exclusion was done to avoid dubious hot-wire measurements in the close vicinity of roughness elements where flow separation may be present, and to ensure the measured flow was always unidirectional. The flow parameters were extracted via parameter optimization by non-linear regression fit of the 1-Probe data to theoretical forms (composite function for smooth-wall flow, and a wake fit for rough-wall flow, as presented in Chauhan *et al.* [51]). All measurements were made at a sampling frequency of 70 kHz and a record length of 120 s per wall-normal position, giving a Nyquist frequency, $\Delta t^+ \sim 0.62$ (*superscript* '+' represents wall scaling), and a record length of $\sim 21,000\,\delta/U_\infty$. The inner-scaled length (l^+) of the hot-wire sensing element was ~ 45.

Through the rest of the text, u is used to represent streamwise fluctuating velocity. Subscripts i and o are used to represent *inner* and *outer* probe measurements, while subscript-suffixes L and s are used to refer to *large* and *small* scale components. The variable $R_{x,y}$ represents correlation function between respective sub-scripted quantities, and super-scripts a and f are used to indicate a quantity corresponding to amplitude modulation and frequency modulation, respectively. For example, u_{iL} represents *inner, large-scale, streamwise velocity time series*, and $R_{oL,iL}$ is given by

$$R_{oL,iL}(\tau) = \frac{\langle u_{oL}^+(t) * u_{iL}^+(t-\tau)\rangle}{\sqrt{\langle u_{oL}^{+2}\rangle\langle u_{iL}^{+2}\rangle}}, \tag{1}$$

where, according to convention given by Eqn. (1), τ indicates a *lead* (if $\tau > 0$) or a *lag* (if $\tau < 0$) of the latter quantity (u_{iL} here) with respect to the former (u_{oL} here) on the time axis.

III. INNER-OUTER INTERACTIONS: 1-PROBE VS 2-PROBE MEASUREMENTS

The inner–outer interactions in a smooth-wall turbulent boundary layer are, in principle, the interactions between (a) the large-scale structures (LSMs and VLSMs) in the logarithmic region and (b) the small scale structures near the wall produced by the 'autonomous' turbulence production cycle. Most experimental studies that have investigated these interactions captured streamwise velocities corresponding to these two flow features acquired by single-component hot-wire anemometry. Various correlations (described later in § IV A) between these two measured velocity signatures measured then quantify the degree of amplitude and frequency modulation present in the flow. Thus, to truly capture these two velocity signatures that reside in distinct regions of the flow, one must make simultaneous measurements at two different wall-normal positions to capture the signatures and quantify the modulating effect of the large-scale motions away from the wall with the small-scale motions near the wall. This is thus the objective of the 2-probe measurements presented herein: to unambiguously capture the velocity signatures of the near-wall and outer-layer structures and quantify their degree of interaction.

However, it should be noted that recent studies in smooth-wall turbulent flows [16] reveal that the large-scale streamwise velocity measured close to wall (u_{iL}) serves as an excellent proxy for the true large-scale signature in the

logarithmic region (u_{oL}). This observation indicates that the large-scale motions away from the wall linearly superpose upon the wall-parallel smaller scales close to the wall. This notion is physically consistent with Townsend's attached eddy hypothesis [32], and was later also shown by Metzger and Klewicki [52] and Hutchins and Marusic [13]. A similar consistency between u_{iL} and u_{oL} was noted in the current smooth-wall, 2-probe measurements which revealed a correlation between the signals [$R_{oL,iL}$, Eqn. (1)] of at least 70%. Thus, the assumption of the 1-probe measurements and associated analysis presented herein, consistent with previous work utilizing 1-probe measurements, assumes that the large-scale velocity signal near the wall is a direct superposition of that which exists in the logarithmic layer (i.e., $u_{iL} \sim u_{oL}$).

However, this assumption that the large scales of log region are linearly superposed on the near-wall velocity signal may not be valid for rough-wall flow. In rough-wall flow, the near-wall, viscous turbulence production cycle of smooth-wall flow is replaced by the roughness-sublayer whose physics is driven directly be interactions between the flow and the roughness topography. At high Re, this is an inertia-dominated process owing to vortex shedding from the roughness features and so the population of near-wall smaller-scales could be dramatically different in character and in subsequent interaction with the larger-scale motions that reside far from the roughness. While previous studies have shown the presence of outer-layer structures in rough-wall flows where the roughness is small compared to the outer length scale of the flow (i.e., $\delta/k \gg 1$), it cannot be assumed *a priori* that these larger-scale motions will linearly superpose their signatures on the velocity signal within the roughness sublayer as has been shown in smooth-wall flow. Thus, to appropriately quantify the degree of true interaction between the larger-scale motions in the outer region with the smaller-scale motions in the roughness sublayer, these two velocity signatures must be independently captured in rough-wall flow and a true 2-point analysis of this correlation is required. In this regard, the current 2-point measurements allowed quantification of the degree of similarity between u_{iL} and u_{oL} for the rough-wall flow, and while still relatively high, it is certainly less significant than in smooth-wall flow ($R_{oL,iL}|_{RW} \approx 50\%$). Finally, it should be noted that the superposition of the large scales on the near-wall region is not instantaneous, i.e., there is a time lag between the occurrence of an 'event' in the log region, and its imprint near the wall. This effect highlights subtle differences in correlations observed in 1-probe and 2-probe analyses, particularly via a time shift, τ. This effect will be elaborated in later sections, when results from the two methods are compared.

IV. AMPLITUDE MODULATION

A. Analysis

Amplitude modulation between the small- and large-scale velocity fluctuations in turbulent boundary layers has been investigated using various methods in earlier studies. All of these methods involve, as a first step, decomposing time series velocity data into small- and large-scale components (u_s and u_L, respectively) using an appropriate cut-off frequency (f_c). This decomposition is followed by identifying a representative measure to quantify the amplitude of the small scales. Observing the correlation between the large scales and such quantified 'amplitude' changes hence reveal any AM effects of the former on the small scales.

Bandyopadhyay and Hussain [15] and Guala *et al.* [22] have investigated the amplitude modulation as the correlation between the large scales (u_L) and the large-scale component of the small-scale velocity magnitude ($[|u_s|]_L$)– the latter obtained via the aforementioned cut-off frequency, f_c. A similar analysis can be performed using the large-scale variance of the small scales ($[u_s^2]_L$) [29]. Ganapathisubramani *et al.* [29] have also reported changes in small-scale variance with the magnitude of the large scales using conditional averaging instead of correlations. A more common approach introduced by Mathis *et al.* [16, 17] utilizes a Hilbert transform to investigate AM effects. Recent work of Baars *et al.* [1] used continuous wavelet transforms (CWT) to obtain time–frequency spectrograms of the time-series data, and integrating the energy at scales below f_c gave a measure of small-scale energy. Correlations can then be examined to observe AM interactions. More details of this last technique, albeit for frequency modulation investigations, will be presented in § V (the reader is referred to Baars *et al.* [1] for a more details). All of these approaches have shown qualitatively similar results in earlier studies corresponding to AM effects in smooth-wall turbulent boundary layers.

The current work uses the Hilbert Transform method, first employed by Mathis *et al.* [16]. 1-probe and 2-probe correlation coefficients ($R^a_{u_{iL},E_L[u_{is}]}, \equiv R^a_{1P}$ and $R^a_{u_{oL},E_L[u_{is}]}, \equiv R^a_{2P}$ respectively) between the large scales and the large-scale envelope of small scales are presented to investigate the amplitude modulation effects. Further, following Mathis *et al.* [17], a fixed cut-off wavelength of $\lambda_c^+ = 7000$ at all wall-normal locations is used to separate small and large scales (The wavelength (λ_c) is transposed into frequency domain (f_c) by using the local mean velocity and Taylor's frozen field hypothesis). Previous studies [16] report the qualitative features of the correlation coefficients to be insensitive to the exact value of the cut-off frequency (f_c) chosen, so long as it 'adequately' separates the near-wall small scales from the large scales in the outer layer. This insensitivity to cut-off wavelength was confirmed in the

current work. Since our interest herein lies in a phenomenological nature of the inner–outer interactions in rough-wall flow, and not on the scaling aspects of the same, a similar cut-off wavelength was found justified as it adequately separates the small scales from the very large scales based on the energy spectra (shown later in Fig. 4). For the current rough-wall flow, since the energy of the roughness-generated flow scales resides at small wavelengths since $k \ll \delta$, a cut-off wavelength based on any of the roughness scales is not appropriate for this purpose. The reader is directed to the aforementioned references for further details on the 1- and 2-probe amplitude modulation analysis procedure.

In the coming discussion, pre-multiplied spectrograms of the streamwise TKE ($k\phi_{uu}$) are also presented to show the energy distribution among different scales as a function of wall-normal position. A frequency integral of this spectrum for a given wall-normal location recovers the corresponding variance of the streamwise velocity fluctuation signal.

B. 1-Probe: AM effects in smooth-wall flow

From the data acquired from the 1-probe experiments, the pre-multiplied spectrogram ($k\phi_{uu}$) and the associated AM correlation map (R_{1P}^a) for smooth-wall data is shown in Fig. 3. These spectra and correlation characteristics are consistent with that previously reported for smooth-wall flow in various earlier studies [1, 16, 22, 23, 30, to name a few], and the important observations have been consolidated here for the sake of completeness and contextual relevance to the rough-wall results.

Both of these results highlight a few important features of the smooth-wall turbulent boundary layer. First, the pre-multiplied spectrogram (Fig. 3a) clearly shows the inner peak in TKE production at $y^+ \sim 15$ and $\lambda_x^+ \sim 1500$. However, in addition to this peak, an additional peak in TKE is noted in the outer layer, corresponding to the energetic VLSMs at $y^+ \sim 200 \,(\equiv 3.9\sqrt{\delta^+})$ and $\lambda \sim 9\delta$, as seen in Ng $et\ al.$ [8].

Figure 3b presents the 1-probe AM correlation map, R_{1P}^a, for smooth-wall flow. Three distinct regions can be observed in this correlation result. The wake region ($\lambda > 0.7\delta$, region III in Fig. 3b) has a prominent anti-correlation peak near ($y = \delta$, $\tau^+ = 0$), implying that every time a positive large-scale velocity is measured, a simultaneous ($\tau^+ = 0$) reduction in small-scale energy is observed, and vice versa. This behavior can be attributed to the intermittency in the wake region of the flow associated with large-scale entrainment, wherein a higher velocity comes from a free stream packet (of low turbulence) being entrained, and lower velocity comes from the turbulent fluid ejected from the near-wall region [30]. As one would expect, this feature is absent in internal flows (pipes and channels, [53]) where this free-stream intermittency is absent under fully-developed flow conditions. Apart from this outer peak in the wake region, a symmetric correlation–anti-correlation peak (region II in Fig. 3b), centered about the y-location of the aforementioned VLSM peak [$y^+ \sim 200 \,(\equiv 3.9\sqrt{\delta^+})$], is observed in the inertial region. This feature can be interpreted as a symmetric arrangement of small scales around the inclined larger-scale structures (LSMs and VLSMs), as seen, for example, in Hutchins $et\ al.$ [24] and Chung and McKeon [23]. Duvvuri and McKeon [20, 54] have further analyzed this structural organization and receptivity to external forcing and is attributed to arrangement of the small scales relative to the large scales. Finally, the near-wall region ($y^+ < 25$, region I in Fig. 3b) contains a single dominant peak, indicating a small-scale energy that is correlated with the corresponding large scale measured, and so with a positive time delay (τ^a). As discussed in previous studies, we consider only this correlation peak to be an indication of true inner–outer interactions, distinct from the scale arrangement and intermittency effects in the inertial and wake regions of the flow, respectively. In other words, the correlation coefficient used to evaluate inner-outer interactions, i.e., R_{1P}^a, can additionally capture other phenomena, such as preferential arrangement of small scales and intermittency. This observation is further discussed in the corresponding frequency modulation correlation maps presented in § V.

C. 1-Probe: AM effects in rough-wall flow

Figure 4 shows the pre-multiplied spectrograms and 1-probe AM correlation maps for the rough-wall boundary layer at spanwise locations corresponding to a low momentum pathway (LMP, $left$) and high-momentum pathway (HMP, $right$) [See Fig. 1]. The spectrograms for the LMP and HMP positions (Figs. 4a and 4b, respectively) show that the near-wall turbulence production peak is destroyed by the presence of roughness and is replaced with a different energy distribution in the roughness sublayer. In contrast, the outer regions of both spectrograms are qualitatively similar to one-another (LMP and HMP) and to smooth-wall flow (Fig. 3a). This consistency is in accordance with the notion of outer-layer similarity wherein the outer flow adapts in a universal manner and the roughness simply sets the wall shear and the outer length scale (when $\delta \gg k$). In this regard, the energy magnitudes at various scales are expected to scale according to the local conditions, such as δ and Re as reported in Table I. These large scale spanwise heterogeneities in TKE are reported in more detail in Barros [47].
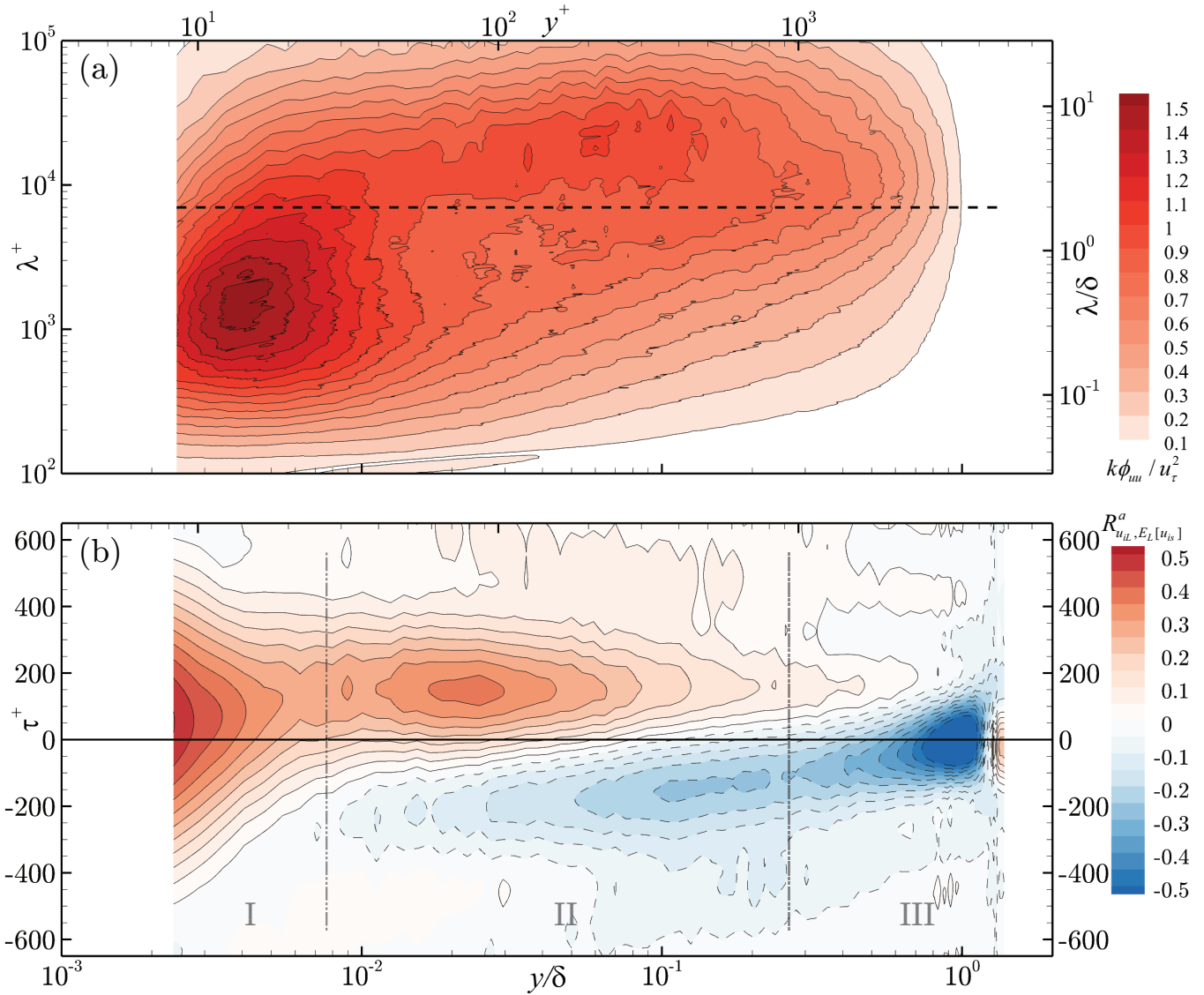
FIG. 3. (a) Pre-multiplied streamwise TKE spectrogram (dashed horizontal line corresponds to $\lambda_x^+ = 7000$– the cut-off wavelength) and (b) single-point AM correlation coefficient, R_{1P}^a (regions I, II and III marked in the correlation map) for smooth-wall flow.

In the AM correlation maps for the LMP and HMP positions (Figs. 4c and 4d, respectively), outer-layer similarity is also evident in the current rough-wall flow. Of noted difference compared to the smooth-wall correlation, there exists a significant overlap between the inner-region modulation and the inertial-region scale arrangement in the rough-wall flow. This overlap makes it more difficult to clearly demarcate the aforementioned regions I and II, as was done in smooth-wall flow (Fig. 3b). This overlap is particularly severe in the LMP region compared to the HMP result. Nevertheless, the magnitude of the correlation coefficient close to the wall does indicate the presence of AM influences similar to that of smooth-wall flow, though the wall-normal extent of this AM region is ambiguous owing to the above mentioned overlap.

The degree of AM is more clearly seen in zero-time-delay correlation coefficients ($R_{1P}^a|_{\tau=0}$) that are more commonly reported in the literature [16]. Figure 5 presents wall-normal profiles of $R_{1P}^a|_{\tau=0}$ for the two rough-wall cases along with the smooth-wall result for comparison. The high degree of AM of the small scales within the roughness sublayer by the large scales is clearly evident and, in fact, *exceeds* that of smooth-wall flow until $y \approx 0.15 - 0.2\delta$. Beyond this wall-normal position, the two rough-wall correlation coefficients (LMP and HMP) collapse with the smooth-wall result, further supporting outer-layer similarity in the current rough-wall flow with smooth-wall behavior far from the roughness as previously reported by Wu and Christensen [34] based on single- and two-point turbulence statistics. The fact that this AM diagnostic is higher in rough-wall flow than its smooth-wall counterpart is interesting given
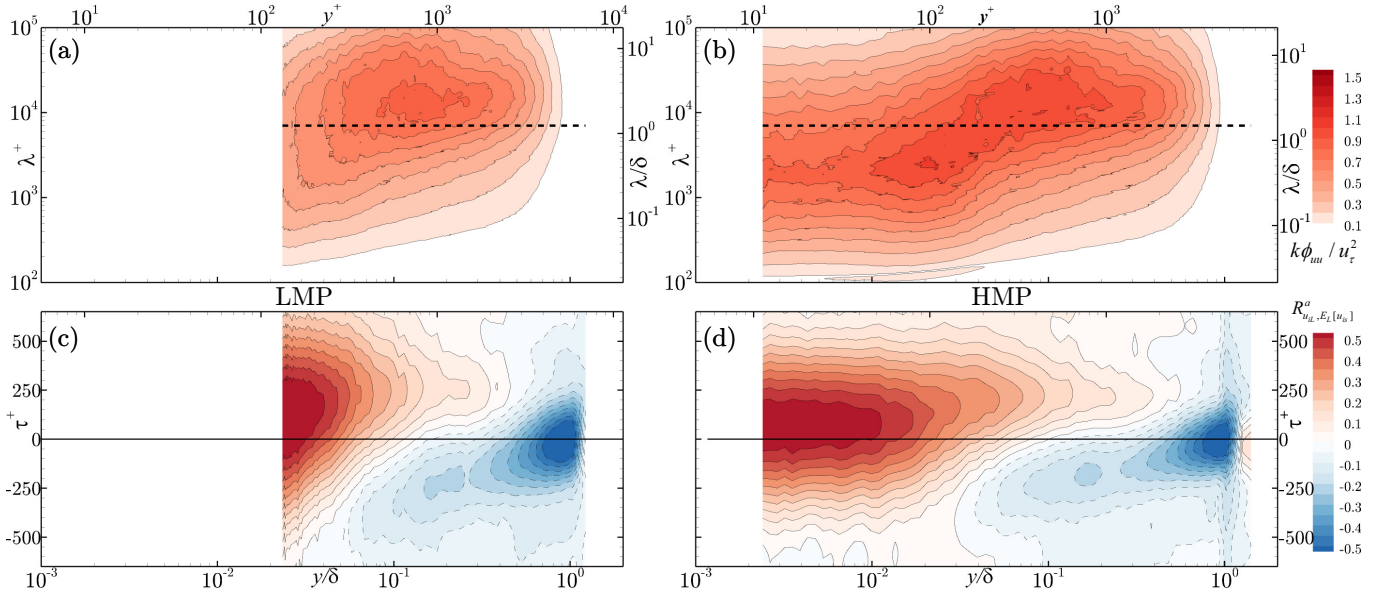
FIG. 4. (a, b) Pre-multiplied streamwise TKE spectrograms (dashed horizontal line corresponds to $\lambda_x^+ = 7000$– the cut-off wavelength) and (c, d) single-point AM correlation coefficients, R_{1P}^a, for rough-wall flow at an LMP and a HMP, respectively.
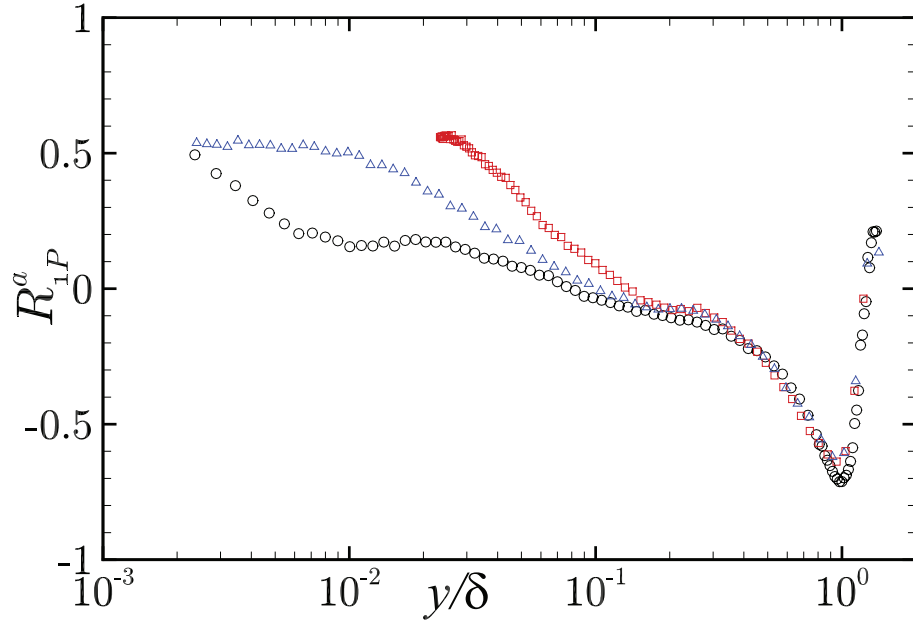

FIG. 5. The zero-time-delay AM correlation coefficient, $R_{1P}^a|_{\tau=0}$, as defined by Mathis *et al.* [16], as a function of the wall-normal position. $\bigcirc$: smooth; $\square$: Rough (LMP); $\triangle$: Rough (HMP).

that roughness disrupts the near-wall turbulence production cycle that correlates well with the outer larger scales in smooth-wall flow. However, this increased AM correlation level is observed from the 1-probe measurements, which correlate large scales and small scales locally. Thus, local large scales could be a collective influence of outer-layer superposition and of the scales imparted by the roughness itself. The presence of enhanced AM in this context thus speaks to the strength of these phenomena, and its importance in rough-wall flows.
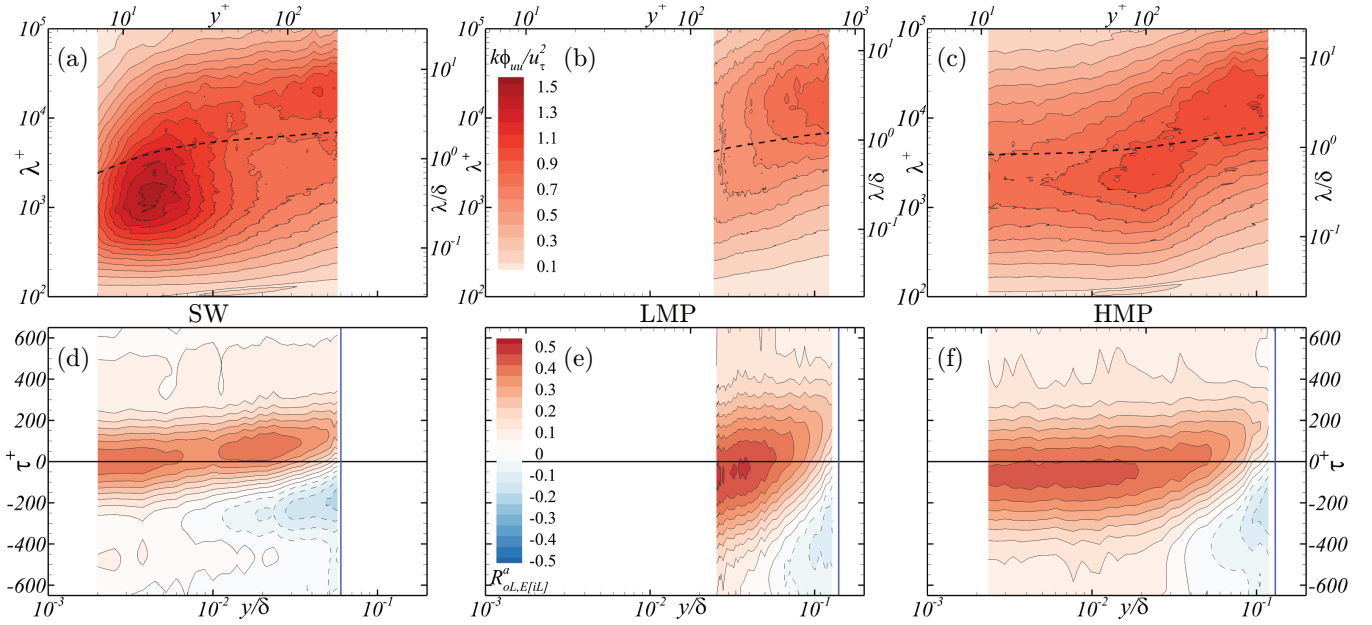
FIG. 6. (a–c) Pre-multiplied streamwise TKE spectrograms (dashed horizontal line corresponds to $\lambda_x^+ = 7000$– the cut-off wavelength) and (d–f) two-point AM correlation coefficients, R_{2P}^a, for smooth- and rough-wall flow at an LMP and a HMP, respectively. The *blue* lines in (d–f) indicate the location of the outer probe for each case.

D. 2-Probe: AM effects

As introduced earlier, the 2-probe measurements unambiguously capture the large scales that reside in the outer region and small scales in the near-wall region, thus allowing direct evaluation of inner–outer interactions. The 2-probe analysis also provides a crucial confirmation that the enhanced AM effects noted in the 1-probe analysis of the rough-wall flow is due to true inner–outer interactions. Further, this 2-probe analysis allows confirmation that the 1-probe AM effects noted in both flows are not merely a manifestation of velocity skewness in the near-wall region [21, 55], but represent actual interaction. Figures 6a–6c show the pre-multiplied spectrograms and correlation maps for the three cases: smooth-wall flow and the rough-wall flow at LMP and HMP locations, respectively. These pre-multiplied spectrograms are computed from the inner-probe data, and should be identical to their 1-probe counterparts. The cut-off filter indicated by the dashed curve in Fig. 6 appears distorted due to the difference in convection velocities used for converting to the two measures of streamwise wavelength: λ^+ (vertical axis in Fig. 6a–6c) and λ_c^{2P} (*dashed* line in Fig. 6a–6c). While the former utilizes the local mean velocity (for consistency with reported spectra in the literature and Fig. 3), the latter uses the constant mean velocity measured by the outer probe.

The AM correlation maps from the 2-probe measurements presented in Figs. 6d–6f confirm the presence of AM effects in the two rough-wall cases as the correlation coefficient is of significant magnitude within the roughness sublayer. Though these 2-probe results show overall similarities with their 1-probe counterparts, a few subtle differences are also noted. In particular, the time delay for maximum correlation that occurs near the wall is quite different between the 1-probe and 2-probe analyses. As discussed earlier in § IV A, the superposition of the inertial region large scales on the near-wall region occurs with a scale-dependent time delay, Δt [24], i.e., a large scale event detected in the logarithmic region occurs near the wall after a time Δt. In an attached eddy framework, this phenomenon can be viewed as measuring *a large scale that is inclined towards the downstream direction, and is convecting past the measurement point*. So, for a fixed streamwise location (as is the case for the probes in the current study), the large scale would be detected by the outer probe earlier (by time Δt) than the lower probe. Thus, a difference in the time delay for this correlation maximum between the 1-probe and 2-probe results is expected for this reason.

From the time delay (τ^+) for maximum near-wall correlation in the 1-probe analysis (for e.g., Fig. 3), the inner–outer AM interaction seems to occur ahead of the superposition of the large scales close to the wall (i.e., $\Delta t > 0$). However, the delay for maximum near-wall correlation from 2-probe analysis is found to be less than that observed in the 1-probe analysis. Figure 7 presents this difference in the time lags clearly, as determined for 1-probe and 2-probe analyses. For smooth-wall flow, the near-wall AM appears at roughly the same time as the outer large scale is detected in the 2-probe result, but a time τ^a earlier than the detection of the near-wall large scale in the 1-probe analysis. Further, in the rough-wall cases, the sign of τ^a is reversed, implying that the outer probe detects the large scale ahead
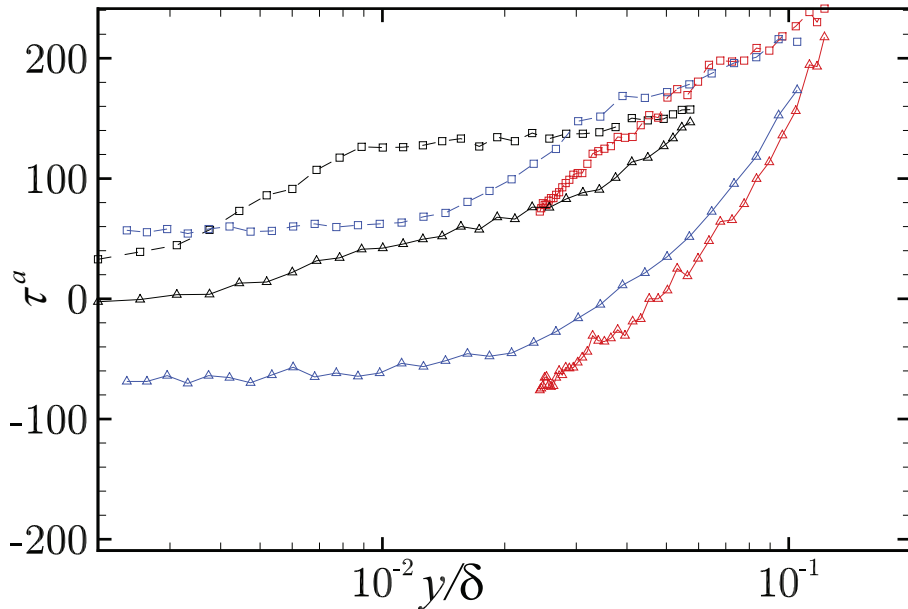
FIG. 7. Time delay for maximum AM correlation coefficient. $\square$: 1-probe; $\triangle$: 2-probe. Smooth; Rough (LMP); Rough (HMP).

of the corresponding AM in the near-wall region. This reversing was not due to the difference in convection velocities used for cut-off wavelength in 1- and 2-probe analysis. Rather, we suspect this delay to depend on the wall-normal location of the outer probe and the structure inclination angle in the inertial region (as is discussed in § VI).

V. FREQUENCY MODULATION

A. Analysis

Frequency modulation (FM) in smooth-wall turbulent boundary layers has been investigated in earlier studies by Ganapathisubramani *et al.* [29] and Baars *et al.* [1]. Both of these studies attempted to relate the change in small-scale 'instantaneous frequency' with the large-scale fluctuations in the boundary layer. Ganapathisubramani *et al.* [29] accomplished this analysis by binning short segments of equal duration of large- and small-scale signals. The average 'frequency' of the small scales was then computed by counting the number of local maxima and minima occurring per segment, and was conditionally averaged on the magnitude of the corresponding large scales. It was shown that the 'average frequency' of the small scales was higher when a positive large-scale fluctuation occurred locally. Alternatively, Baars *et al.* [1] used continuous wavelet transforms (CWT) to perform a time-correlation method for quantifying FM effects, akin to the AM analysis performed in the previous section. The latter CWT method is used herein to investigate FM effects. While a comprehensive description of this method is given in the original work [1], relevant details of the analyses performed in the current study are summarized herein.

The continuous wavelet transform (CWT, $\tilde{u}(t', s)$) of a time series ($u(t)$) involves convoluting the signal with a 'mother wavelet' function, $\psi(t/s)$, as

$$\tilde{u}(t', s) = \frac{1}{\sqrt{s}} \int_{-\infty}^{\infty} u(\tau) \psi\left(\frac{\tau - t'}{s}\right) d\tau. \tag{2}$$

The independent variables of the CWT are the translation, t', and the dilation scale, s. A CWT decomposes a signal $u(t)$ into a time–frequency space, $\tilde{u}(t', f)$, thus identifying various frequency components in the signal at various times. Following Baars *et al.* [1], Fig. 8 shows the pre-multiplied wavelet power spectrum $[f\tilde{E}(t, f)]$ of an illustrative velocity time series segment, that can be computed from the CWT as
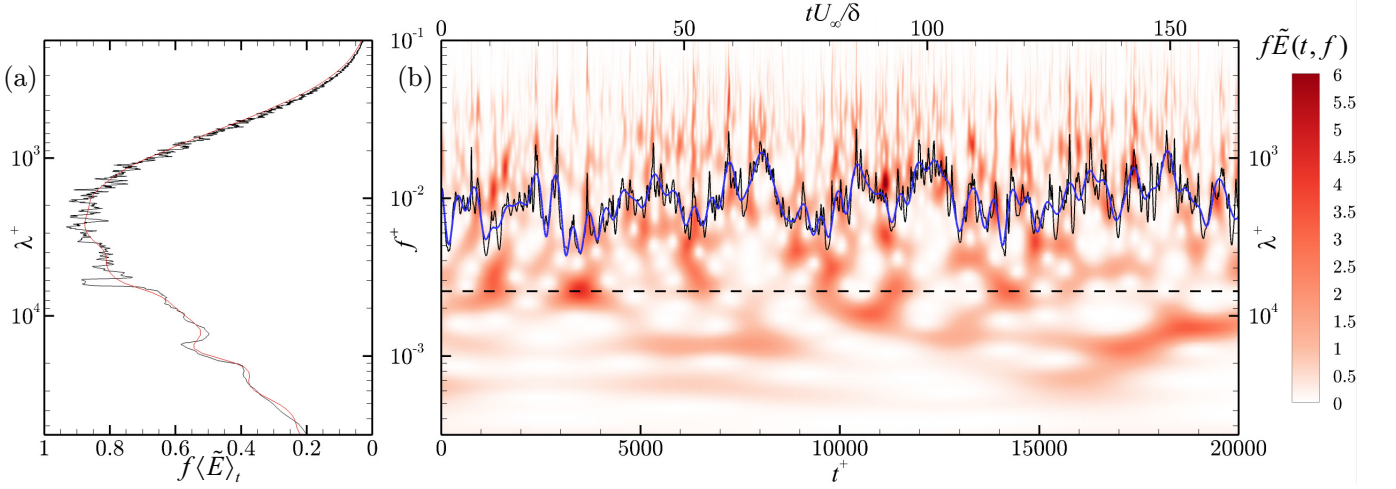
$$\tilde{E}(t, f) = |\tilde{u}(t, f)|^2. \tag{3}$$

FIG. 8. Pre-multiplied wavelet power spectrum ($f\tilde{E}$, *right*) of a velocity time series measured over smooth-wall flow at $y^+ = 9$. The time series on the plot mark the corresponding instantaneous frequencies, f_s and f_{sL}, and the cut-off frequency, f_c (*dashed*). The time average of the WPS ($f\langle\tilde{E}\rangle_t$) is compared with corresponding smoothed pre-multiplied power spectrum ($k\phi_{uu}$) on the *left*–both of which are measures of average distribution of energy among various scales.

The wavelet power spectrum (WPS) at a given time t is thus analogous to an *instantaneous* power spectral density.

For the current work, analytic Morlet wavelet was used as the mother wavelet, and 128 logarithmically spaced scales were resolved, with the smallest scale corresponding to the Nyquist frequency (f_N) and the largest scale corresponding to $\lambda_x = 30\delta$. Also demarcated on the WPS in Fig. 8 are the large scales ($< f_c$) and the small scales ($> f_c$), using the cut-off wavelength (λ_c). The integral of the WPS at frequencies greater than f_c for each time, t, gives a small-scale energy time series [$\sigma_s(t)$, Eqn. (4)], which can also be used in lieu Hilbert transformed envelope signal for AM, as mentioned in § IV A and shown originally by Baars *et al.* [1]. A representative small-scale-frequency signal (or instantaneous frequency signal) can now be defined from the WPS. Following Baars *et al.* [1], the first moment of the small-scale energy distribution at each time is used herein as the instantaneous frequency, $f_s(t)$, that can be computed as

$$f_s(t) = 10^{F(t)} \tag{4}$$

$$F(t) = \frac{1}{(\sigma_s(t))^2} \int_{f_c}^{f_N} \log_{10}(f)\left(f\,\tilde{E}\right) d\log_{10}(f)$$

$$\sigma_s(t) = \left[\int_{f_c}^{f_N} f\,\tilde{E}\,d\log_{10}(f)\right]^{\frac{1}{2}}$$

The instantaneous frequency signal (f_s) and the filtered (at f_c) large-scale component (f_{sL}) are also shown in in Fig. 8. The fluctuating part (f_s') of f_s gives a measure of small-scale frequency changes with time.

Using Eqn. (2), cross-correlation coefficients can be computed between the inner large scales (u_{iL}) and the large-scale frequency fluctuations of small scales (f_{sL}') for quantifying FM effects from 1-probe data. Similar correlation coefficients between the large scales in the outer region (u_{oL}) and the inner frequency fluctuations (f_{sL}') allows quantification of FM effects from 2-probe data, similar to the 2-probe AM analysis summarized earlier. The correlation functions we shall be investigating will be $R^f_{u_{iL},f_{sL}'}(\equiv R^f_{1P})$ for 1-probe, and $R^f_{u_{oL},f_{sL}'}(\equiv R^f_{2P})$ for 2-probe measurements.

B. FM correlation coefficients

Figure 9 presents the 1-probe FM correlation maps for smooth- and the two rough-wall cases (LMP and HMP). The smooth-wall results agree well with the findings of Baars *et al.* [1] which confirms the fidelity of the analysis procedure utilized herein. Further, by contrasting the smooth-wall FM (Fig. 9a) and AM (Fig. 3b) correlation maps, there exist some important similarities and differences. First, the anti-correlation structure observed in the AM result at $y \sim \delta$
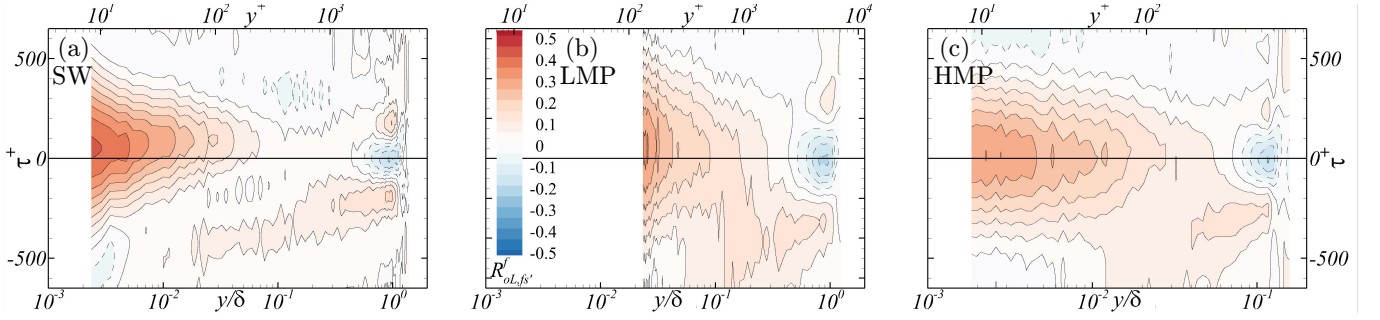
FIG. 9. 1-probe FM correlation maps, R_{1P}^f, for (a) smooth and (b, c) rough-wall flow at an LMP and a HMP, respectively.

owing to wake region intermittency is also present in FM correlation map. However, the correlation–anti-correlation structure that marked the inertial region in the AM result, owing to small-scale arrangement around inertial region large scales (Region II in Fig. 3b), is absent in the FM correlation map for smooth-wall flow (Fig. 9a). Finally, a near-wall peak appears close to the wall in the smooth-wall FM result (Fig. 9a), representing the FM of the near-wall scales by the large scales measured at the same wall-normal location (as this result is from 1-probe analysis). Thus, this result supports the occurrence of modulation in the near-wall region of smooth-wall flow and that this modulation is restricted to the near-wall region.

The rough-wall FM correlation maps (Figs. 9b and 9c for LMP and HMP, respectively) show a similar anti-correlation in the wake region to their 1-probe AM counterparts. However, the ambiguity in the rough-wall AM correlation maps (Fig. 3b) in distinguishing between the inertial region structure (in region II) from the near-wall modulation peak (in region I) is absent in the rough-wall FM correlation maps. This indicates that the FM analysis is a more robust diagnostic for discerning the occurrence of inner–outer interactions, as opposed to simply scale arrangement, compared to AM analysis.

The FM in both the smooth- and rough-wall cases is readily apparent in Fig. 10, which presents the FM correlation coefficient for zero time delay ($R_{1P}^f|_{\tau=0}$) plotted in Fig. 9–the counterparts to the AM correlation profiles in Fig. 5. The two rough-wall FM correlations collapse well for all wall-normal locations until very close to the surface ($y \lesssim 0.04\delta$), where they seem to plateau (~ 0.3) to a lesser value than that of smooth-wall (~ 0.4). Below this location, the FM correlation at the LMP increases sharply while the FM correlation at the HMP increases slowly, with both well-exceeding the smooth-wall result in the near-wall region until the HMP result crosses below the smooth-wall one at $y \approx 0.01\delta$. While the smooth-wall result becomes zero for $y > 0.05\delta$ until the wake region, where the correlation becomes negative owing to wake intermittency, the two rough-wall cases show non-zero correlation much further into the outer region and remain so until $y \approx 0.4\delta$ where they both collapse with the smooth-wall correlation profile through the wake region. This latter behavior could be a consequence of the roughness sublayer occupying a larger portion of the boundary layer (usually taken as $\sim 3 - 5k$, which would be $y \lesssim 0.13 - 0.22\delta$) compared to the buffer layer of the smooth-wall flow ($y \lesssim 0.02\delta$), and thus perhaps a larger inner region being modulated by outer-layer effects. However, these results must be interpreted with caution as, similar to the 1-probe AM correlation coefficients, these results show the interaction between the small scales in the near-wall region with the large-scale signature at the same wall-normal location. Thus, particularly in the rough-wall cases, these local large-scale signatures may not be only from the outer layer but could also include near-wall larger scales that are attributable to roughness.

The 2-probe FM correlation maps, correlating the outer region large scales, u_{oL}, with the sublayer instantaneous frequency, f'_{sL}, are shown in Fig. 11. As noted from the 1-probe and 2-probe AM correlation maps, the 2-probe FM correlation coefficients shows qualitatively similar results to their 1-probe counterparts (Fig. 9) with subtle structural differences. Apart from clear strong FM correlation in the near-wall regions of the smooth- and rough-wall cases (with similar magnitude correlation in the two rough-wall cases but less than the smooth-wall case), these correlation maps reiterate the negative time delay for the maximum correlation ($\tau^f < 0$) between f'_{sL} and u_{oL}. It is interesting to note that two independent measures of inner–outer interaction, both AM and FM, indicate such a time delay, with this negative time delay exclusively observed in the two rough-wall cases. As was mentioned in § IV, this phenomenon likely relates to the inclination of the large-scale outer structure, which will be further discussed in section VI. But apart from these subtle differences, the 1-probe and 2-probe FM results agree well, and establish the occurrence of FM inner–outer interactions in the presence of the roughness considered herein.
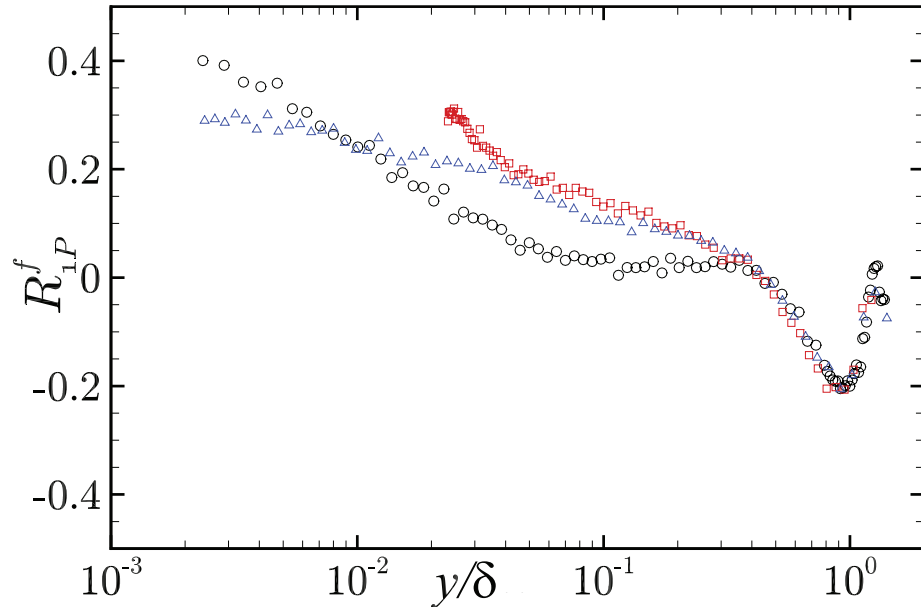
FIG. 10. The zero-time-delay FM correlation coefficient, $R^f_{1P}|_{\tau=0}$, as a function of the wall-normal position. ◯: smooth; □: Rough (LMP); △: Rough (HMP).
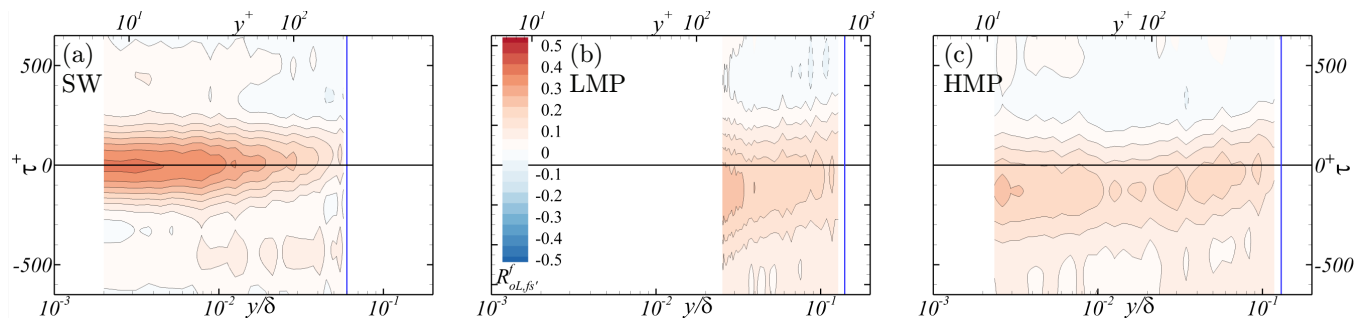

FIG. 11. 2-probe FM correlation maps, R^f_{2P}, for (a) smooth and (b, c) rough-wall flow at an LMP and a HMP, respectively. The *blue* lines indicate the location of the outer probe for each case.

VI. DISCUSSION

The AM and FM correlation coefficients presented, both the 1- and 2-probe representations, provide indications of inner–outer interactions in the rough-wall flow, though these statistical measures must be interpreted appropriately. For example, the amplitude modulation coefficient (R^a), by definition, is only a correlation. As was discussed in § IV (and the literature cited therein), this AM correlation not only embodies inner–outer interactions very close to the wall, but also captures the preferential arrangement of small scales around large-scale events in the outer region of the flow. Of interest here is how this phenomenon might impact interpretation of the rough-wall results presented where there appears to be a stronger overlap, or blurring of the boundary between the near-wall modulation and the inertial-layer scale arrangement. This overlap is absent in all of the FM correlation maps (including the smooth-wall case), though this diagnostic does capture the wake intermittency that is also present in the AM metric.

With this in mind, the AM and FM correlation diagnostics indicate the presence of modulation in the rough-wall flow considered herein. In this regard, it is very interesting to observe that such a strong correlation appears across the rough-wall boundary layer in a manner similar to smooth-wall flow despite the viscous near-wall cycle of the latter being replaced by a roughness sublayer ($k^+ \approx 200$). This observation lends additional support to the mechanism proposed in recent literature [1, 24, 30, 31]–that the near-wall mechanisms perceive these large-scale changes from the outer region as 'instantaneous changes in Re', and adapt quickly to these conditions ('QSQH Hypothesis'). In other
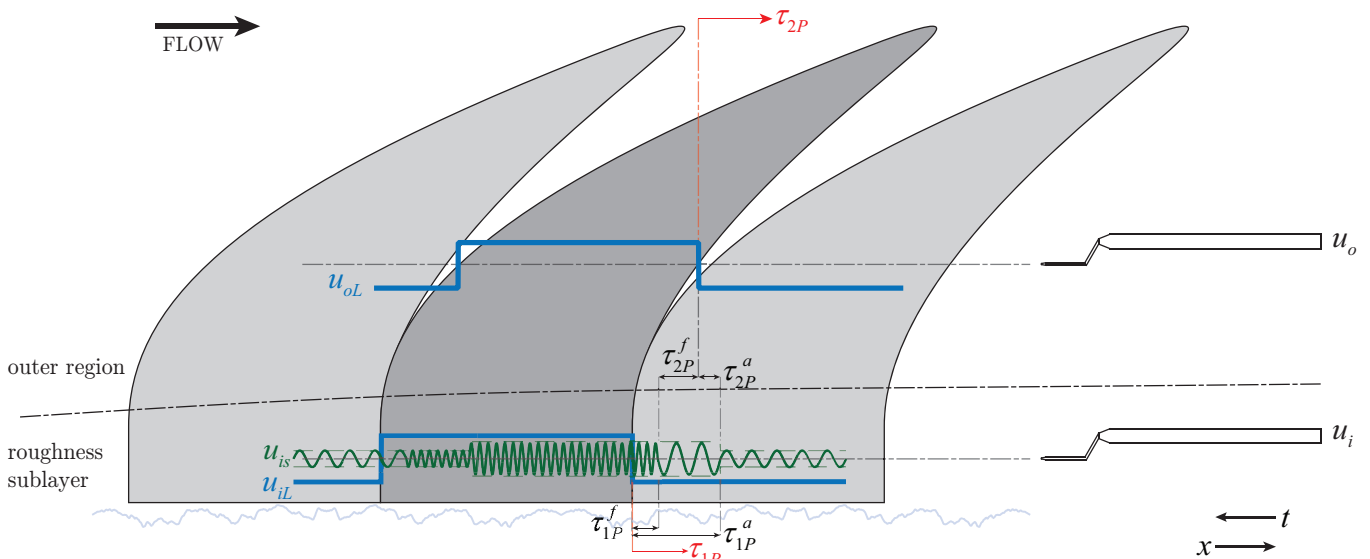
FIG. 12. A schematic representation of inner–outer interactions that was originally presented by Baars *et al.* [1], but modified to represent the current experiments and observations.

words, a high velocity (relative to the mean flow) large-scale event is perceived by the near-wall region as an increase in Re, leading to an increase in small-scale fluctuations and frequency, and vice versa. This proposition follows from the argument that the time scales of evolution of the small scales [$\sim O(t^* \equiv y^*/u_\tau)$] are much smaller than those of the large-scale events [$\sim O(t_h = \delta/U_\infty)$], given sufficient scale separation [which is only achieved at high Re where $y_* \ll \delta$, which translates to large Re_τ ($\equiv \delta/y_*$)]. If this were true, then one would expect the same to also hold in high-Re rough-wall turbulent boundary layers, where the near-wall small scales would similarly experience only the conditions imparted by the large-scale motions away from the wall, and thus amplitude and frequency modulation should appear from similar (if not identical) mechanisms involved in smooth-wall flows. The observations presented herein support this possibility, where the inner–outer interactions appear in a similar fashion, adding support for the aforementioned mechanism. However, it remains to be seen if the scale-wise receptivity/response of the near-wall small scales to the large-scale fluctuations is similar, particularly in rough-wall flows that can, in principle, have a wider range of near-wall scales owing to the presence of a broad range of topographical scales as in the roughness considered herein.

In addition to the 1-probe analysis, the availability of 2-probe measurements provides additional perspective in trying to more fully understand these inner–outer interaction mechanisms. It should be recalled that in a smooth-wall flow, the near-wall large scales of wall-parallel motions are simply a superposition of inertial region large scales, but with a time delay. This notion is confirmed given the qualitative consistency between smooth-wall 1-probe and 2-probe results, such as the structure of the correlation maps etc. In this regard, the small-scale amplitude and frequency modulations from a 1-probe perspective generally lead (in time) the occurrence of the correlated large-scale event. This phenomenon was shown well schematically in Baars *et al.* [1] (see Fig. 12 therein). However, the current 2-probe results for smooth-wall flow indicate that the small-scale amplitude and frequency fluctuations are approximately in phase with the large scales measured in the inertial region (i.e., $\tau_{2P,SW}^a, \tau_{2P,SW}^f \approx 0$). Thus, the occurrence of a large scale at the outer probe and the modulation of the small scales detected by the inner probe seem instantaneous. Though we suspect that this 'instantaneousness' is, in some sense, an artifact of the current location of the outer probe (y_o^+), it is clear that the modulation influences of large scales lead their superposition onto the near-wall region.

With the above understanding of inner–outer interactions, we seek to address the apparent differences between the smooth- and rough-wall results presented herein. Though rough-wall AM and FM correlation coefficients show similar magnitudes and wall-normal trends to that of smooth-wall flow, the time delay between the large scales and the near-wall modulation effects show differences. Since these influences are correlated with respect to the large scales (at $\tau = 0$), let the time delay for maximum AM at any wall-normal position be $\tau^a(y^+)$ and its FM counterpart be $\tau^f(y^+)$. In other words, τ^a and τ^f indicate times by which the modulation influences *lead* or *lag* the large scales (if > 0 or < 0, respectively), as given by the time delay associated with the peak in the respective correlation coefficient.

In this context, consider the schematic in Fig. 12, reproduced from Baars *et al.* [1] but adjusted for the current rough-wall scenario. For smooth-wall flow (in Fig. 3 and Baars *et al.* [1]), it was seen that $\tau_{1P}^a > 0$ and $\tau_{1P}^f > 0$,

implying that the modulation influences lead the local large scales. By virtue of the inclination of the large scales towards the downstream, the detection of a large scale at a higher y^+ location (say y_o^+) occurs at an earlier time relative to the local large scales (since $y^+ < y_o^+$). Hence, one would expect the time delay associated with maximum modulation to be smaller, i.e., $\tau_{2P}^a < \tau_{1P}^a$ and $\tau_{2P}^f < \tau_{1P}^f$. The smooth-wall correlation results clearly reflect this notion (Figs. 7 and 11). In contrast, the negative values of τ_{2P}^a and τ_{2P}^f for the rough-wall cases possibly stem from the outer probe residing farther away from the wall compared to the smooth-wall case. The inclined nature of the large-scale motions results in an even earlier detection by the outer probe relative to the modulation influences near the wall, and hence a lead relative to the latter. The uncertainties in the exact values of these correlation peaks, corrupted in part by the filter roll-off characteristics, limit precise quantification of these delays as a relative motion. However, the trends, and the possible physical explanation for the same, are unambiguous.

VII.   SUMMARY

Recent quantification of inner–outer interactions in wall turbulence via amplitude and frequency modulation suggests that their importance increases with increasing Re, meaning such effects are important to a range of practical flow scenarios that often occur at high Re. Given that such applications occur at high Re, they also often suffer from roughness effects wherein even small surface imperfections can lead to modifications of the near-wall flow behavior (particularly drag and heat-transfer characteristics) as the viscous length scale becomes smaller than the size of these surface imperfections (i.e., the latter begin to protrude from the viscous sublayer). Thus, there exists a need to explore the characteristics of inner–outer interactions via AM and FM in rough-wall flow so that the applicability of such phenomena can be faithfully extended to practical flow scenarios. The experiments reported herein serve this specific purpose as the occurrence of AM and FM is explored in a high-Re turbulent flow overlying a complex roughness topography replicated from a turbine blade damaged by deposition of foreign materials. This surface serves as a proxy for that encountered in practical flow scenarios wherein surface roughness is often multi-scale and irregular in nature. Previous studies have shown roughness-induced secondary flows to exist in the mean flow over this topography, reflected in the occurrence of low- and high-momentum pathways (LMP and HMP, respectively) alternating in the spanwise direction [43–45]. Thus, the current rough-wall measurements were made coincident with each of these mean-flow features to explore similarities and differences in the inner–outer interactions along these pathways.

The primary observation in the current work is that modulation influences are present in the rough-wall flow at both LMP and HMP locations. In particular, there exist strong similarities in the AM correlation maps for smooth- and rough-wall flow, including strong near-wall correlation indicative of modulation, inertial-region small-scale arrangement around large scales, and wake intermittency, all of which further support previous observations of outer-layer similarity in the current rough-wall flow [34, 35, 41]. However, unlike smooth-wall flow where there exists a clear separation between the near-wall modulation signature and the inertial-region scale arrangement, the rough-wall results show ambiguity in this regard.

The FM correlation maps also show strong similarities between the smooth- and rough-wall cases, further supporting the occurrence of strong modulation of the near-wall small scales by the large scales in the outer region. However, as previously reported by Baars *et al.* [1], FM analysis captures near-wall modulation influences while avoiding ambiguity from inertial-layer scale arrangement (in contrast to AM analysis) which assisted in confirming the occurrence of near-wall modulation in the two rough-wall cases. Finally, the 2-probe measurements presented herein provided a direct measure of the large scales in the outer region which allowed unambiguous diagnosis of inner–outer interactions, as assumptions related to similarities and imprints of the outer large scales within the roughness sublayer were not required (as is typically assumed and previously confirmed in smooth-wall flow).

The similarity of these inner–outer interactions between the smooth- and rough-wall flows is striking. The near-wall small scales seem to respond to outer-layer large scales, irrespective of how the former are generated, i.e., from the viscous turbulence production cycle of smooth-wall flow or from vortex shedding by roughness elements that creates a roughness sublayer that entirely replaces the viscous sublayer. Further, as was shown in § VI, the modulation of small scales as measured by the correlation coefficient is invariant of where the large scales are sampled. While this observation is trivial in smooth-wall flow, the fact that this is even valid in rough-wall flow re-emphasizes the similarity of inner–outer interactions between the two flows that have very different near-wall flow characteristics. This observation means that, at least for the current rough-wall flow, 1-probe measurements, with subsequent assumptions about how the outer large scales superimpose upon the near-wall region, are sufficient to observe the basic modulation phenomena. The results presented herein also indicate that FM is a less ambiguous diagnostic of inner–outer interactions compared to AM, especially for the current rough-wall flow wherein near-wall modulation and inertial-region scale arrangement could not be separated in AM analysis. Finally, the current observations tend to agree with the mechanisms proposed by Hutchins [30] and Baars *et al.* [1], where the small scales, irrespective of their generation mechanism, respond in a quasi-steady way to changes in the outer-layer structure.

[1] W.J. Baars, K.M. Talluru, N. Hutchins, and I. Marusic, "Wavelet analysis of wall turbulence to study large-scale modulation of small scales," Exp. Fluids **56**, 1–15 (2015).

[2] F. H. Clauser, "The turbulent boundary layer," Adv. Appl. Mech. **4**, 1–51 (1956).

[3] S.J. Kline, W.C. Reynolds, F.A. Schraub, and P.W. Runstadler, "The structure of turbulent boundary layers," J. Fluid Mech. **30**, 741–773 (1967).

[4] J. Jiménez and A. Pinelli, "The autonomous cycle of near-wall turbulence," J. Fluid Mech. **389**, 335–359 (1999).

[5] R. L. Panton, "Overview of the self-sustaining mechanisms of wall turbulence," Progress in Aerospace Sciences **37**, 341–383 (2001).

[6] K.C. Kim and R.J. Adrian, "Very large-scale motion in the outer layer," Phys. Fluids **11**, 417–422 (1999).

[7] B.J. Balakumar and R.J. Adrian, "Large-and very-large-scale motions in channel and boundary-layer flows," Phil. T. Roy. Soc. A **365**, 665–681 (2007).

[8] H.C.H. Ng, J.P. Monty, N. Hutchins, M.S. Chong, and I. Marusic, "Comparison of turbulent channel and pipe flows with varying Reynolds number," Exp. Fluids **51**, 1261–1281 (2011).

[9] N. Hutchins and I. Marusic, "Evidence of very long meandering features in the logarithmic region of turbulent boundary layers," J. Fluid Mech. **579**, 1–28 (2007).

[10] K.T. Christensen and R.J. Adrian, "Statistical evidence of hairpin vortex packets in wall turbulence," J. Fluid Mech. **431**, 433–443 (2001).

[11] B. Ganapathisubramani, E.K. Longmire, and I. Marusic, "Characteristics of vortex packets in turbulent boundary layers," J. Fluid Mech. **478**, 35–46 (2003).

[12] V. K. Natrajan and K. T. Christensen, "The role of coherent structures in subgrid-scale energy transfer within the log layer of wall turbulence." Phys. Fluids **18**, 065104 (2006).

[13] N. Hutchins and I. Marusic, "Large-scale influences in near-wall turbulence," Phil. T. Roy. Soc. A **365**, 647–664 (2007).

[14] K.N. Rao, R. Narasimha, and M.A. Narayanan, "The bursting phenomenon in a turbulent boundary layer," J. Fluid Mech. **48**, 339–352 (1971).

[15] P. R. Bandyopadhyay and A.K.M.F. Hussain, "The coupling between scales in shear flows," Phys. Fluids **27**, 2221–2228 (1984).

[16] R. Mathis, N. Hutchins, and I. Marusic, "Large-scale amplitude modulation of the small-scale structures in turbulent boundary layers," J. Fluid Mech. **628**, 311–337 (2009).

[17] R. Mathis, N. Hutchins, and I. Marusic, "A predictive inner–outer model for streamwise turbulence statistics in wall-bounded flows," J. Fluid Mech. **681**, 537–566 (2011).

[18] I. Marusic, W. J. Baars, and N. Hutchins, "An extended view of the inner-outer interaction model for wall-bounded turbulence using spectral linear stochastic estimation," Procedia Eng. **126**, 24–28 (2015).

[19] R. Mathis, I. Marusic, N. Hutchins, and K.R. Sreenivasan, "The relationship between the velocity skewness and the amplitude modulation of the small scale by the large scale in turbulent boundary layers," Phys. Fluids **23**, 121702 (2011).

[20] S. Duvvuri and B.J. McKeon, "Triadic scale interactions in a turbulent boundary layer," J. Fluid Mech. **767**, R4 (2015).

[21] M. Bernardini and S. Pirozzoli, "Inner/outer layer interactions in turbulent boundary layers: a refined measure for the large-scale amplitude modulation mechanism," Phys. Fluids **23**, 061701 (2011).

[22] M. Guala, M. Metzger, and B.J. McKeon, "Interactions within the turbulent boundary layer at high reynolds number," J. Fluid Mech. **666**, 573–604 (2011).

[23] D. Chung and B.J. McKeon, "Large-eddy simulation of large-scale structures in long channel flow," J. Fluid Mech. **661**, 341–364 (2010).

[24] N. Hutchins, J.P. Monty, B. Ganapathisubramani, H.C.H. Ng, and I. Marusic, "Three-dimensional conditional structure of a high-reynolds-number turbulent boundary layer," J. Fluid Mech. **673**, 255–285 (2011).

[25] I. Jacobi and B.J. McKeon, "Phase relationships between large and small scales in the turbulent boundary layer," Exp. Fluids **54**, 1–13 (2013).

[26] K.M. Talluru, R. Baidya, N. Hutchins, and I. Marusic, "Amplitude modulation of all three velocity components in turbulent boundary layers," J. Fluid Mech. **746**, R1 (2014).

[27] R. Mathis, I. Marusic, S. I. Chernyshenko, and N. Hutchins, "Estimating wall-shear-stress fluctuations given an outer region input," J. Fluid Mech. **715**, 163–180 (2013).

[28] D. Fiscaletti, B. Ganapathisubramani, and G.E. Elsinga, "Amplitude and frequency modulation of the small scales in a jet," J. Fluid Mech. **772**, 756–783 (2015).

[29] B. Ganapathisubramani, N. Hutchins, J.P. Monty, D. Chung, and I. Marusic, "Amplitude and frequency modulation in wall turbulence," J. Fluid Mech. **712**, 61–91 (2012).

[30] N. Hutchins, "Large-scale structures in high reynolds number wall-bounded turbulence," in *Progress in Turbulence V* (Springer, 2014) pp. 75–83.

[31] C. Zhang and S. I. Chernyshenko, "Quasisteady quasihomogeneous description of the scale interactions in near-wall tur-

bulence," Phys. Rev. Fluids **1**, 014401 (2016).

[32] A. A. Townsend, *The structure of turbulent shear flow* (Cambridge University Press, 1976).

[33] M.R. Raupach, R.A. Antonia, and S. Rajagopalan, "Rough-wall turbulent boundary layers," Appl. Mech. Rev. **44**, 1–25 (1991).

[34] Y. Wu and K.T. Christensen, "Outer-layer similarity in the presence of a practical rough-wall topography," Phys. Fluids **19**, 85108–85108 (2007).

[35] Y. Wu and K. T. Christensen, "Spatial structure of a turbulent boundary layer with irregular surface roughness," J. Fluid Mech. **655**, 380–418 (2010).

[36] R. Mejia-Alvarez, Y. Wu, and K.T. Christensen, "Observations of meandering superstructures in the roughness sublayer of a turbulent boundary layer," Int. J. Heat Fluid Fl. **48**, 43–51 (2014).

[37] D.T. Squire, W.J. Baars, N. Hutchins, and I. Marusic, "Inner–outer interactions in rough-wall turbulence," Journal of Turbulence **17**, 1159–1178 (2016).

[38] K. Blackman and L. Perret, "Non-linear interactions in a boundary layer developing over an array of cubes using stochastic estimation," Physics of Fluids **28** (2016).

[39] M. Nadeem, J. H. Lee, J. Lee, and H. J. Sung, "Turbulent boundary layers over sparsely-spaced rod-roughened walls," Int. J. Heat Fluid Flow **56**, 16–27 (2015).

[40] W. Anderson, "Amplitude modulation of streamwise velocity fluctuations in the roughness sublayer: evidence from large-eddy simulations," J. Fluid Mech. **789**, 567–588 (2016).

[41] R. Mejia-Alvarez and K.T. Christensen, "Low-order representations of irregular surface roughness and their impact on a turbulent boundary layer," Phys. Fluids **22**, 015106 (2010).

[42] R. Mejia-Alvarez and K.T. Christensen, "Wall-parallel stereo particle-image velocimetry measurements in the roughness sublayer of turbulent flow overlying highly irregular roughness," Phys. Fluids **25**, 115109 (2013).

[43] J.M. Barros and K.T. Christensen, "Observations of turbulent secondary flows in a rough-wall boundary layer," J. Fluid Mech. **748**, R1 (2014).

[44] D. Willingham, W. Anderson, K. T. Christensen, and J. M. Barros, "Turbulent boundary layer flow over transverse aerodynamic roughness transitions: Induced mixing and flow characterization," Phys. Fluids **26**, 025111 (2014).

[45] W. Anderson, J. M. Barros, and K. T. Christensen, "Numerical and experimental study of mechanisms responsible for turbulent secondary flows in boundary layer flows over spanwise heterogeneous roughness," J. Fluid Mech. **748**, 316–347 (2015).

[46] R. Mejia Alvarez, *Experimental study of low-order models of highly-irregular roughness and their impact on turbulent boundary layers*, Ph.D. thesis, University of Illinois at Urbana-Champaign (2011).

[47] J. Barros, *Cross-plane stereo-PIV measurements of a turbulent boundary layer over highly irregular roughness*, Ph.D. thesis, University of Illinois at Urbana-Champaign (2014).

[48] B. Nugroho, N. Hutchins, and J.P. Monty, "Large-scale spanwise periodicity in a turbulent boundary layer induced by highly ordered and directional surface roughness," Int. J. Heat Fluid Flow **41**, 90–102 (2013).

[49] Kevin, J.P. Monty, H.L. Bai, G. Pathikonda, B. Nugroho, J.M. Barros, K.T. Christensen, and N. Hutchins, "Cross-stream stereoscopic piv of a modified turbulent boundary layer over directional surface pattern," (manuscript submitted for publication) (2016).

[50] P. H. Alfredsson and R. Örlü, "The diagnostic plot?a litmus test for wall bounded turbulence data," Euro. J. Mechanics-B/Fluids **29**, 403–406 (2010).

[51] K. Chauhan, H. Nagib, and P. Monkewitz, "On the composite logarithmic profile in zero pressure gradient turbulent boundary layers," in *Proc. 45th AIAA Aerospace Sciences Meeting, Paper No. AIAA*, Vol. 532 (2007) pp. 1–18.

[52] M.M. Metzger and J.C. Klewicki, "A comparative study of near-wall turbulence in high and low reynolds number boundary layers," Phys. Fluids **13**, 692–701 (2001).

[53] R. Mathis, J. P. Monty, N. Hutchins, and I. Marusic, "Comparison of large-scale amplitude modulation in turbulent boundary layers, pipes, and channel flows," Phys. Fluids **21**, 111703 (2009).

[54] S. Duvvuri and B. McKeon, "Nonlinear interactions isolated through scale synthesis in experimental wall turbulence," Phys. Rev. Fluids **1**, 032401 (2016).

[55] P. Schlatter and R. Örlü, "Quantifying the interaction between large and small scales in wall-bounded turbulent flows: A note of caution," Phys. Fluids **22**, 051704 (2010).

[56] M. Alfred, *Signal Analysis Wavelets, Filter Banks, Time-Frequency Transforms and Applications* (John Wiley and Sons, New York, 1999).

[57] C. Torrence and G. P. Compo, "A practical guide to wavelet analysis," Bulletin of the American Meteorological society **79**, 61–78 (1998).